Near-field Ion Current Density Measurements of a 6-kW Hall Thruster

IEPC-2009-124

Presented at the 31st International Electric Propulsion Conference,
University of Michigan • Ann Arbor, Michigan • USA
September 20 – 24, 2009

Bryan M. Reid[1] and Alec D. Gallimore[2]
University of Michigan, Ann Arbor, MI 48109, USA

Abstract: Faraday probe measurements were taken in the near-field plume of a 6-kW Hall thruster to reduce the negative effects of facility-induced charge-exchange collisions. The results from these measurements were analyzed using a non-standard definition of the current density integration bounds that produced self-consistent beam current and beam divergence values. The measurements indicated a beam divergence half-angle of 16° and an ion beam fraction of 0.78 at the thruster's nominal operating condition of 300 V and 20 mg/s. These global parameters were used in a probe-based efficiency architecture and the resulting anode efficiency matched thrust stand measurements within 3.2% (absolute not relative). These results represent a marked improvement over traditional far-field Faraday probe measurements that grossly over-predict beam current and beam divergence.

Nomenclature

CEX	=	charge-exchange	$I_{tot,dyn}$	=	dynamic integration beam current
$D_{T,mean}$	=	thruster mean diameter	j	=	ion current density
I_b	=	ion beam current	OR	=	outer radius
I_d	=	discharge current	r	=	radial location
IR	=	inner radius	η_b	=	current utilization
I_{tot}	=	total integrated beam current	η_d	=	divergence utilization
$I_{tot,DC}$	=	discharge channel beam current	θ	=	divergence half angle

I. Introduction

As Hall thrusters gain popularity in the spacecraft propulsion community it is becoming more important to understand major efficiency loss mechanisms. The anode efficiency can be broken into five utilizations (loss mechanisms): voltage, charge, mass, current, and divergence [1]. The voltage and charge utilizations have a value of approximately 0.95 for high-efficiency Hall thrusters [2-3]. They are measured with a Retarding Potential Analyzer and E×B probe, respectively. The mass utilization is not directly measured and is essentially a combination of the current and charge utilizations, having a value of approximately 0.90 for xenon propellant [2-3]. The remaining two utilizations (current and divergence) are typically measured with a far-field Faraday probe and normally have the highest degree of uncertainty associated with them. A Faraday probe measures the distribution of ion current density throughout the plume and the results are analyzed to determine the ion beam current and far-field plume divergence half-angle. The beam current calculated from these far-field measurements often exceeds the discharge current,

[1] Currently a member of the Technical Staff at MIT Lincoln Laboratory Optical Systems Engineering Group, b.reid@ll.mit.edu. Research performed as a doctoral candidate at the Plasmadynamics and Electric Propulsion Laboratory at the University of Michigan.
[2] Arthur F. Thurnau Professor of Aerospace Engineering and Director of the Plasmadynamics and Electric Propulsion Laboratory, alec.gallimore@umich.edu.

which violates Kirchhoff's current law. The beam current is used to determine the current utilization efficiency using

$$\eta_b = \frac{I_b}{I_d}, \tag{1}$$

where I_b is the ion beam current and I_d is the discharge current. The beam divergence half-angle calculated from far-field faraday probes typically exceeds 40° and the corresponding divergence utilization is

$$\eta_d = (\cos\theta)^2, \tag{2}$$

where θ is the divergence half-angle. Equation 2 indicates that the maximum achievable efficiency is approximately 60% at θ = 40° before any other losses are included. Since Hall thrusters can achieve > 60% anode efficiency as measured by a thrust stand (includes all plasma-related losses), this gross over-prediction of beam divergence is one of the most flawed measurements included in probe-based efficiency analyses.

One of the primary reasons for the poor measurement of beam current and beam divergence is the negative effect of facility-induced Charge-EXchange (CEX) collisions. These collisions cause a re-distribution of main beam ions into the periphery of the plume, artificially increasing the measured beam divergence. This re-distribution of charge also contributes to the over-estimation of beam current since ions collected at the periphery of the plume are weighted higher in the hemispherical integration. To reduce the effect of facility-induced CEX, current density measurements were taken close to the exit plane of a 6-kW Hall thruster to reduce the probability that a main beam ion will encounter a CEX collision prior to reaching the probe. These measurements were taken within approximately one thruster diameter downstream of the thruster, a region often referred to as the near-field plume. A similar experiment was performed by Hofer *et al*. [4] and Jameson *et al*. [5] with promising results. However, neither of these experiments provided self-consistent measurements of both beam current and beam divergence. The work in this paper attempts to address these limitations.

II. Experimental Apparatus

This section describes the vacuum facility, Hall thruster, and probe used for the near-field current density measurements. The near-field Faraday probe description includes probe design, data collection, beam current and plume divergence calculation methods, and sources of uncertainty.

A. Vacuum Facility

Experiments were performed in the Large Vacuum Test Facility (LVTF) at the University of Michigan (UM) Plasmadynamics and Electric Propulsion Laboratory (PEPL). The LVTF is a 6-m-diameter, 9-m-long, cylindrical, stainless steel chamber. Pumping is provided by seven cryo-pumps and liquid nitrogen shrouds, with a nominal pumping speed of 240,000 l/s on xenon. The facility base pressure was approximately 2.3×10^{-7} torr, as measured by two hot cathode ionization gauges. More details on the facility and pressure monitoring equipment can be found in Refs. [6-7].

B. Thruster

Experiments were performed using a 6-kW laboratory model Hall thruster that has an approximate throttling range of 100-600 mN and 1000-3000 s specific impulse [8-11]. The thruster was equipped with a center-mounted LaB_6 hollow cathode that was operated at 7% of the anode mass flow rate. Research-grade xenon propellant (99.999% pure) was supplied to the anode and cathode by separate commercially-available flow meters and controllers, having an accuracy of ± 1% of full scale.

C. Near-field Faraday Probe

1. Probe Design

The collecting surface of the near-field ion current density probe was made of a 4.85-mm-diameter molybdenum disk that was fastened to a tungsten rod through an interference fit. Molybdenum was chosen for its relatively high operating temperature and low secondary electron emission coefficient. The 2-mm-diameter tungsten rod was housed in a 4.80-mm-outer-diameter alumina tube. The probe did not incorporate a guard ring, primarily due to the very small Debye length that required an impractical gap width of < 0.1 mm.

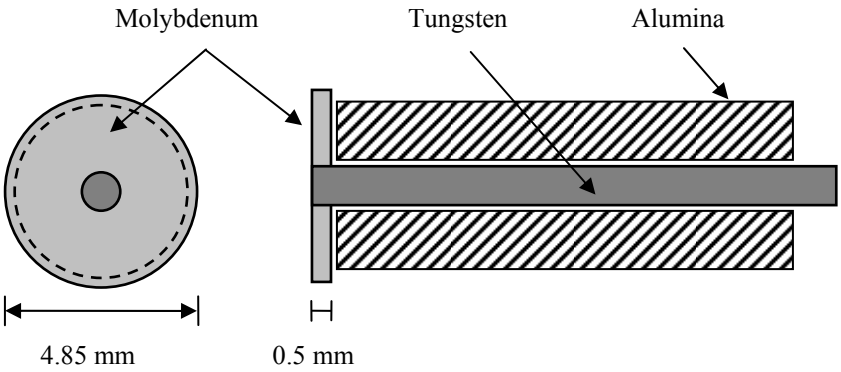

Figure 1 Schematic of near-field Faraday probe design and construction (not to scale).

The probe was biased at -60 V with respect to facility ground (typically 70-80 V below plasma potential) and the current was measured across a 56 Ω thin-film resistor (121 Ω at 30 mg/s). This probe bias was consistent with the results in Ref. [4] that indicated saturation of the collected ion current at approximately -50 V with respect to ground.

2. Data Collection

The probe was actuated using the High-speed Axial Reciprocating Probe (HARP) [12] and data were taken along radial paths that extended from +2.35 to -1.25 mean thruster diameters ($D_{T,mean}$) from thruster centerline. Radial sweeps began at an axial location of 5.25 $D_{T,mean}$ and ended at 0.06 $D_{T,mean}$ from the thruster exit plane. A diagram of the data collection domain is shown in Figure 2.

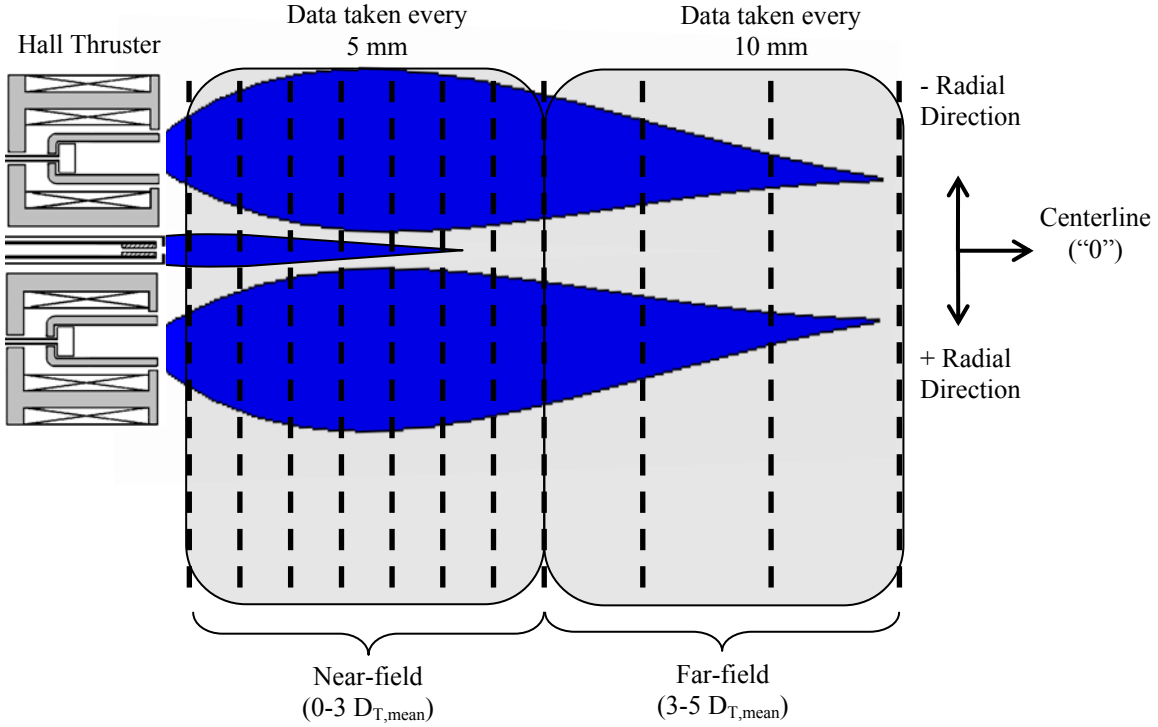

Figure 2 Measurement domain for the near-Faraday probe measurements (not to scale).

The data acquisition system recorded the probe position, ion current density, thruster discharge current, and thruster cathode potential at 100 kHz per channel. This resulted in a distinct measurement of each signal every 0.1 mm in the radial direction and adequately resolved the fluctuation in collected current due to nominal discharge current oscillations at approximately 20 kHz [2].

3. Beam Current Calculation

Traditional beam current calculations were not appropriate for the data collected with the near-field Faraday probe. The primary difference beyond the probe design was that the near-field data were recorded along radial paths rather than along a constant radius arc. This discrepancy changes the integration method from spherical into a cylindrical coordinates. The primary disadvantage of the data collection method proposed in this paper is that in the cylindrical plane, measurements must extend to infinity in the radial direction to capture the entire thruster plume. This impracticality is quickly reached by most facilities and translation stages. Fortunately, the thruster plume is reasonably approximated by a Gaussian distribution (see Figure 3 and discussion below), and as such, the bulk of the plume is contained within a few characteristic diameters. This limitation is further diminished as the probe approaches the exit plane of the thruster.

Since traditional beam current calculations could not be used with these near-field measurements, several beam current integration methods were explored in Ref. [2]. In all cases, the ion beam current was calculated by integrating the current density at each axial location using:

$$I_b = 2\pi \int_{IR}^{OR} j(r) r dr, \tag{3}$$

where $j(r)$ is the axial current density at each radial location r and the plume was assumed axisymmetric. The integration limits in the radial direction (IR and OR) were chosen based on one of three methods:

1) Total current (I_{tot}): Integrate the ion flux from thruster centerline to the maximum radial location (2.35 $D_{T,mean}$). This method is analogous to the hemispherical integration method used in traditional Faraday probe analyses. This method has limited applicability since the integral tends to infinity at large radial locations. In addition, this method produces undesirable results by including slow-moving ions located along thruster centerline that are emitted by the cathode and do not contribute to thrust.

2) Discharge channel integration ($I_{tot,DC}$): Integrate only the ion flux that exists directly downstream of the thruster exit plane between the discharge channel inner and outer radii ($R_{CL} \pm b/2$). This method assumes that all ions exit the discharge channel and travel with zero radial velocity. This method is similar to the one in Ref. [5]; however, its usefulness diminishes as the distance from the exit plane increases due to ion beam broadening (ion-ion and ion-neutral scattering and radial electric fields).

3) Dynamic integration ($I_{tot,dyn}$): Integrate the flux that exists within a window around the peak ion flux, defined as the location where flux drops to 1/e of its maximum value. This method creates an integration width that is consistent with the exit plane near the thruster (also consistent with option 2 above), yet adapts with the axial evolution of the current density distribution to capture the ions in the main beam.

The bounds selection in method 3) was based upon the 1/e cutoff used in the field of physics, especially Gaussian-beam laser optics, where it can represent the radial extent of the laser's peak irradiance. Since the plume of a Hall thruster can be reasonably approximated by a Gaussian, the 1/e cutoff should serve as a reasonable limit. The excellent approximation to a Gaussian is shown in Figure 3 for measurements at 0.06 $D_{T,mean}$. The Gaussian fit was of the form

$$y = y_0 + A \exp\left[-\left(\frac{x - x_0}{width} \right)^2 \right], \tag{4}$$

where $y_0 = 1.9485$, $A = 129.06$, $x_0 = 0.50574$, and $width = 0.095312$. The Gaussian fit is valid throughout most of the near-field plume, but is only valid to approximately ± 15 degrees from centerline at 1 meter downstream (far-field).

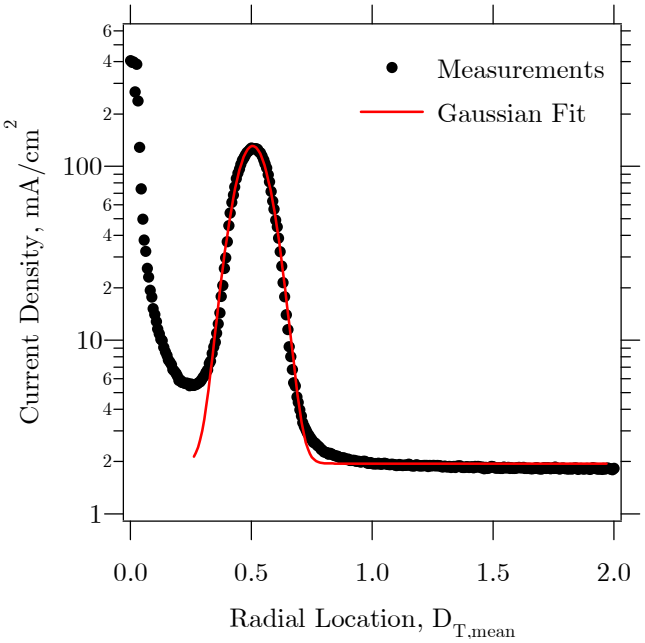

Figure 3 Illustration of the quasi-Gaussian profile of the ion beam at 0.06 $D_{T,mean}$.

4. Plume Divergence Calculation

Without knowledge of the ion velocity field in the plume, the plume divergence angle must be defined based on the location of the primary ion flux (current density). Far-field Faraday probe analysis uses this principle when determining the 90% or 95% plume divergence half angle, which are somewhat arbitrarily defined. These definitions have traditionally produced unreasonably high plume divergence calculations that are inconsistent with performance measurements. This is discussed further in Section IV.C.

Since the beam current was calculated using a 1/e cutoff, the plume divergence was defined as the angle subtended by the 1/e locations. This approach is intuitive; an appropriate analogy is the pattern that a laser pointer produces on a wall. In this situation, a spectator would likely determine the laser's divergence by comparing the size of the beam on the wall with the distance between the laser and the wall. This is exactly the approach used in the near-field Faraday probe analysis of this paper and it is consistent with methods used by laser physicists.

The 1/e beam divergence definition assumes the ion beam is a point source located at the center of the discharge channel exit plane. The validity of this approximation is loosely supported by internal plasma measurements that showed the ion beam was concentrated towards channel centerline and the ion density peaked near the thruster exit [13-14]. Unfortunately, this approximation is not valid within the first few tenths of a mean thruster diameter downstream. This is indicated by unrealistically high calculated beam divergence half-angles close to the thruster (see results in Section IV.B).

These new definitions for beam current and plume divergence represent a drastic change from the standard Hall thruster data analysis methods. The results from these calculations produce superior agreement with efficiency analysis when compared to standard analysis techniques, discussed further in Section IV.C. It should be noted that this beam divergence angle is not calculated directly *from* the ion beam momentum; instead it provides information *about* the ion beam momentum (cosine losses).

5. Sources of Uncertainty

There are two primary sources of uncertainty associated with the near-field probe measurements; collection area and collected current. The collection area can be influenced by probe sheath expansion as the probe is moved away from the thruster exit plane and the probe view factor as the probe is moved away from thruster centerline. The collected current can be influenced by secondary electron emission due to high-energy ion impacts and collection of CEX ions. None of these sources of uncertainty were addressed in this work. Although the final results are encouraging, this does not necessarily indicate that these sources should be neglected in future work. For instance, the effects of sheath expansion could be investigated using concurrent measurements of plasma density and electron temperature. On the other hand, we can easily rationalize that the effect of probe view factors can be neglected since the correction will be small over the areas of interest near channel centerline (*i.e.*, $\cos(10°) = 0.985$). Similarly, the

effect of facility-induced CEX in the near-field (0-2 $D_{T,mean}$) is negligible compared to the contribution from thruster-induced CEX [15]. We will not attempt to correct for thruster-induced CEX since they constitute a natural evolution of the plume, even in vacuum conditions.

The corrections listed above require additional measurements and several underlying assumptions that have the potential to obscure the final results. Instead of attempting to include these sources of uncertainty, we will omit them and opt for conservative ±20% uncertainty bounds for the beam current and plume divergence.

III. Results

To isolate the effect of neutral flow rate, the magnetic field shape, cathode flow fraction, and discharge voltage were kept constant while varying the anode flow rate. The 6-kW thruster was designed for nominal operation at 6 kW (300 V and 20 mg/s), but during this study it was operated at discharge powers ranging from approximately 3 to 10 kW, corresponding to 300 V at 10, 20, and 30 mg/s. Additional measurements were reported at 150 V and 10, 20, and 30 mg/s in Ref. [2].

The applied magnetic field shape was held constant at each operating condition and the strength was optimized for maximum total efficiency. The true magnetic field may have been significantly different due to self-fields induced by the Hall current [16]. It should be noted that the thruster operates at 2-3% higher efficiency at fully optimized magnet settings including an internal trim coil. The pumping speed remained constant at each operating condition, which caused the facility pressure to increase with increasing flow rate. This increased the amount of background neutrals that were ingested by the thruster, which led to higher discharge current [2, 17].

Contours of the near-field ion current density for thruster operation at 300 V and 10, 20, and 30 mg/s are shown in Figure 4. Each contour represents more than 64,000 individual measurements of the local current density. All three contours showed that the ion beam exited the thruster channel and remained highly collimated for the first thruster diameter. Beyond the first thruster diameter, the main ion beam broadened and eventually coalesced near thruster centerline. The location of coalescence moved downstream with increased anode mass flow rate. This was consistent with internal plasma measurements that showed the plasma moved downstream with increasing flow rate [13-14].

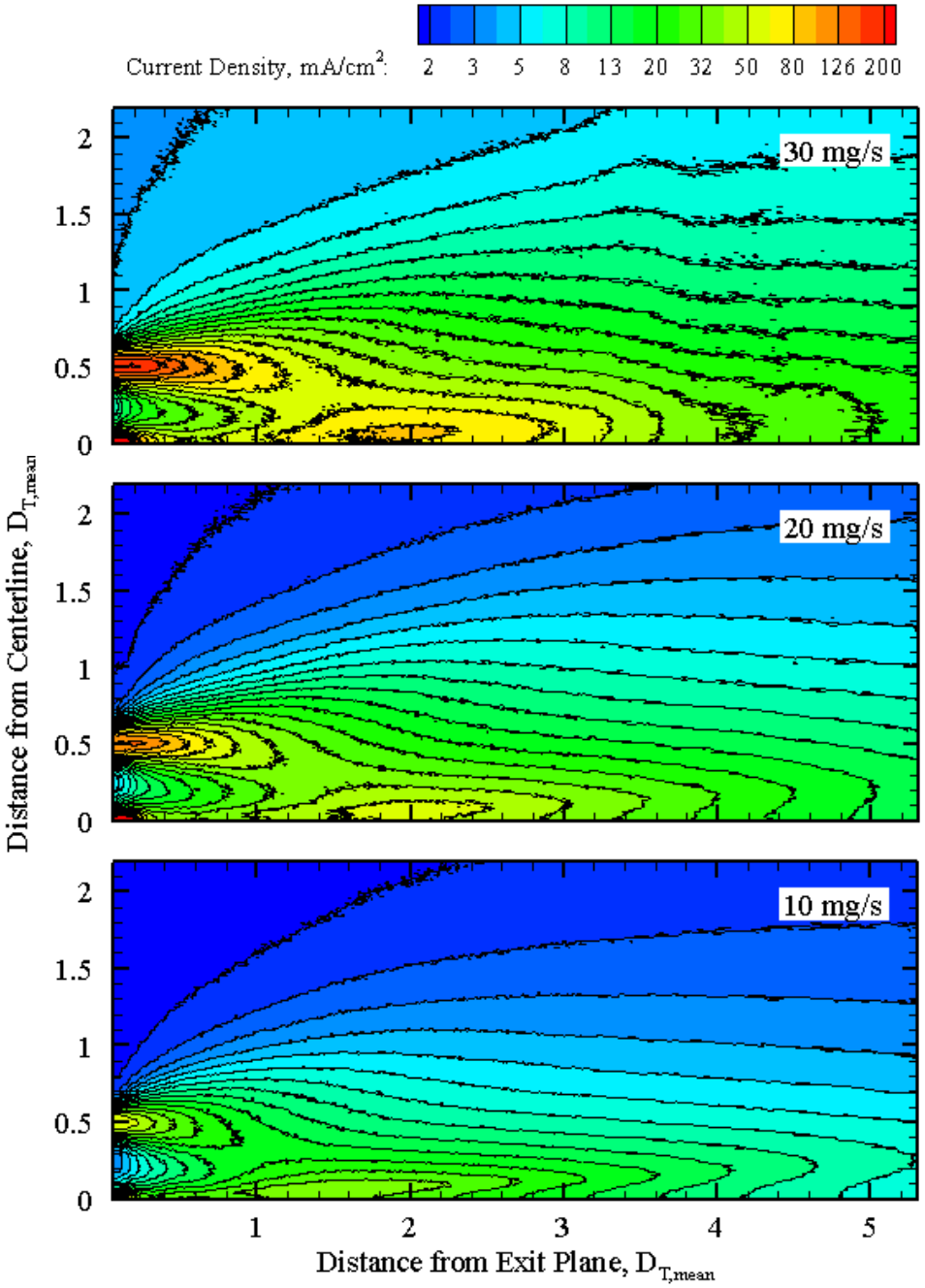

Figure 4 Ion current density in the near-field plume for thruster operating conditions of 300 V and 10, 20, and 30 mg/s (note exponential contour scaling).

Changes in the characteristic shape of the ion current density shown in Figure 4 can be more clearly seen by examining radial traces at several axial locations as shown in Figure 5 for thruster operation at 300 V and 20 mg/s. Near the thruster exit, the current density displayed three peaks; the two outer peaks represented each side of the thruster annulus and the center peak represented the cathode. Further downstream, the magnitude of the cathode peak decreased, ultimately fading into the rest of the profile. This double-peaked profile resembles the shape of a traditional far-field Faraday probe trace.

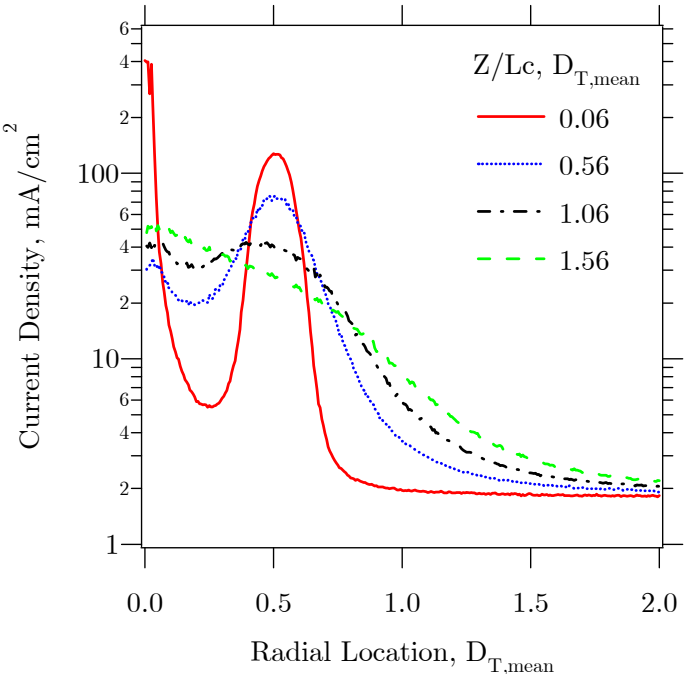

Figure 5 Comparison of ion current density at several axial locations for thruster operation at 300 V and 20 mg/s.

The peak current density as a function of axial distance from the thruster is shown in Figure 6, indicating a modest peak downstream of the thruster exit at 20 and 30 mg/s. The difference between the peak current density and the exit plane current density was larger at 30 mg/s than at 20 mg/s, indicating a dependence on flow rate that may have been attributed to increased collection of CEX ions or increased ingestion of facility neutrals that were ionized and accelerated outside the thruster. These contributions would have a larger impact at higher flow rates due to higher facility pressures.

Another potential contribution to the downstream peak in maximum current density was insufficient probe bias; however, results in Refs. [13-14] indicated that the electron temperature was too low to contribute in this way (T_e < 5 eV). Another contribution may have been additional ion acceleration in the near-field plume that was shown in near-field plasma potential measurements [13-14] and LIF measurements [18-19]. The end of the acceleration region occurred at approximately 0.02, 0.03, and 0.07 $D_{T,mean}$ for thruster operation at 10, 20, and 30 mg/s, respectively. Since these are well upstream of the peak ion current density location of approximately 0.2 $D_{T,mean}$ for 20 and 30 mg/s, the effect of incomplete ion acceleration likely had a relatively small effect. Although the exact cause for the peak in maximum current density downstream of the thruster exit is not known at this time, its existence is the primary reason that calculating the beam current at the exit plane alone is not strictly valid as suggested in Ref. [5].

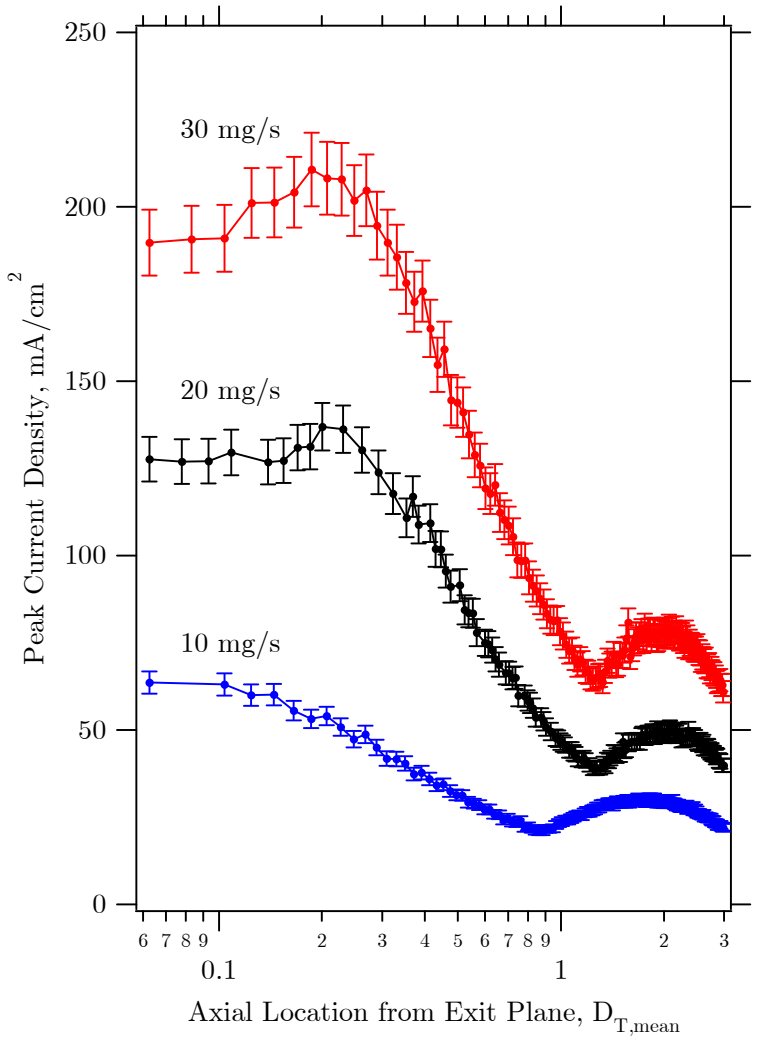

Figure 6 Peak current density for thruster operation at 300 V and 10, 20, and 30 mg/s.

IV. Analysis and Discussion

The results from the previous section are used to determine the beam current and plume divergence. These parameters are ultimately used in an efficiency analysis, and the calculated efficiency is compared to the measured efficiency from a thrust stand. The results are also compared to traditional far-field measurements.

A. Beam Current

The beam current was calculated using all three methods outlined in Section II.C.3, and the results are shown in Figure 7 as a function of axial distance. Integrating the entire current density profile from centerline to the maximum radial location (I_{tot}) resulted in calculated beam currents that were well above the discharge current, similar to the gross over-prediction observed in traditional far-field beam current calculations. Integrating the current density with the discharge channel method ($I_{tot,DC}$) produced calculated beam currents that were approximately 20% below the discharge current near the thruster exit plane; however, the beam current drastically decreased after approximately 0.3 $D_{T,mean}$, restricting the usefulness of the calculation. This limitation was caused by the beam crossing at approximately 1 $D_{T,mean}$ shown in Figure 4. The beam crossing caused the peak current density to be shifted away from channel centerline, resulting in a drastic decrease in the flux of ions located within the static integration domain.

The dynamic window integration method was attractive because it produced a beam width that was approximately equal to the discharge channel exit width at the channel exit plane, while providing a dynamic integration domain that accounted for the effects of beam broadening further downstream. This integration method

produced reasonable beam currents (approximately 20% below the discharge current) that were consistent with the DC-only integration near the thruster. The integrated current from the dynamic technique extended the region of acceptable beam currents from 0.3 to greater than 1 $D_{T,mean}$.

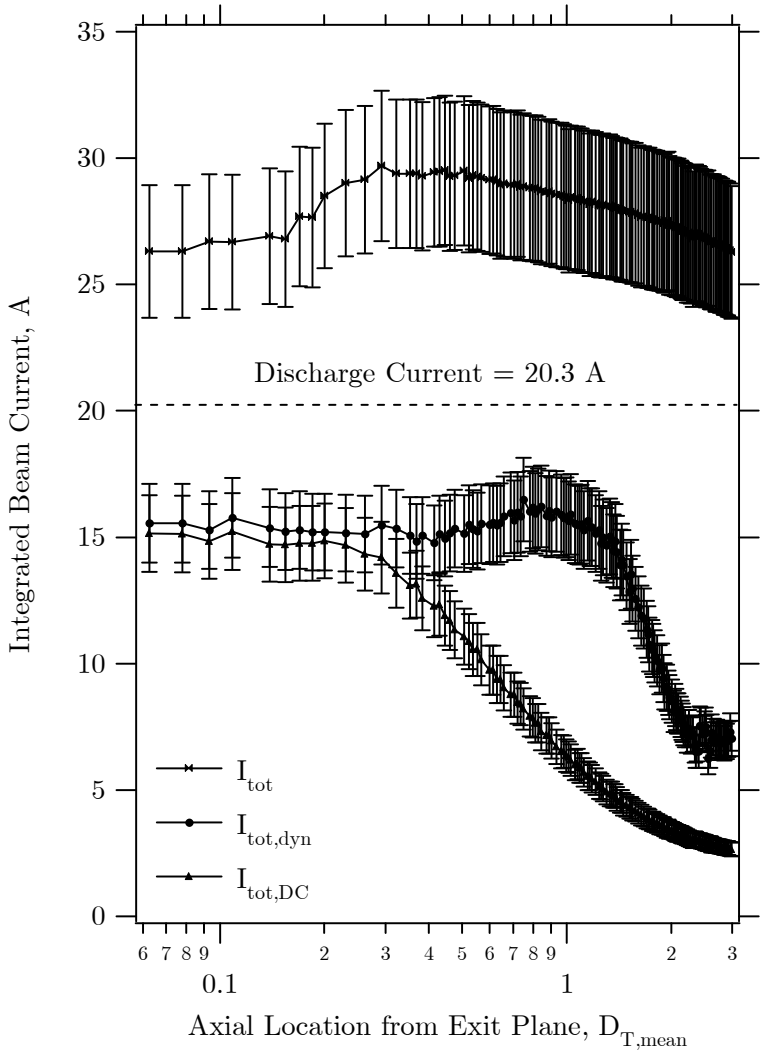

Figure 7 Integrated ion beam currents using three different integration techniques for thruster operation at 300 V and 20 mg/s.

All reported beam current values were calculated from the dynamic window integration method by averaging the beam current from 0.5 to 1.0 $D_{T,mean}$. The beam current calculated at each axial location is shown in Figure 8, having values of 7.35, 15.8, and 25.9 A at 10, 20, and 30 mg/s, respectively. The corresponding ion current fractions (I_b/I_d) were 0.812, 0.777, and 0.766, respectively. The ion current fraction is commonly referred to as the current utilization [1].

B. Plume Divergence

The plume divergence was calculated at each axial location and the results are shown in Figure 9. Since the plume divergence definition approximated the ion beam as a point source, the calculated divergence was unreasonably high near the thruster exit plane. After 0.4 $D_{T,mean}$ downstream (approximately two channel widths), the calculated divergence angle leveled off and remained essentially constant until approximately 1 $D_{T,mean}$. Beyond that point, the calculated divergence angle decreased since the entire plume was not captured because of the limited radial data collection domain. The plume divergence for each operating condition was calculated by taking the average from 0.5 to 1.0 $D_{T,mean}$ (consistent with beam current calculation). The plume divergence was 20°, 16°, and 16° at 10, 20, and 30 mg/s, respectively.

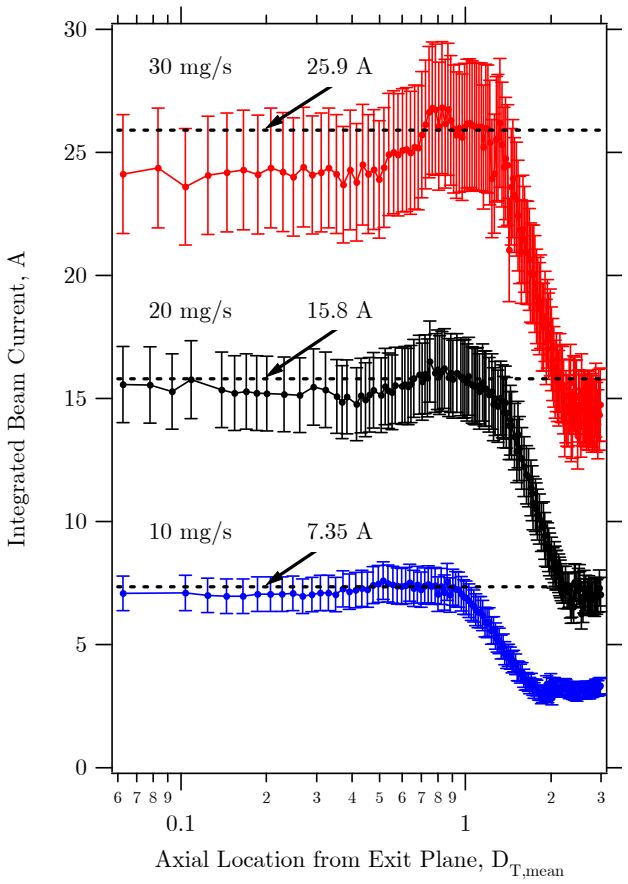

Figure 8 Integrated ion beam current at each axial location for thruster operation at 300 V and 10, 20, and 30 mg/s.

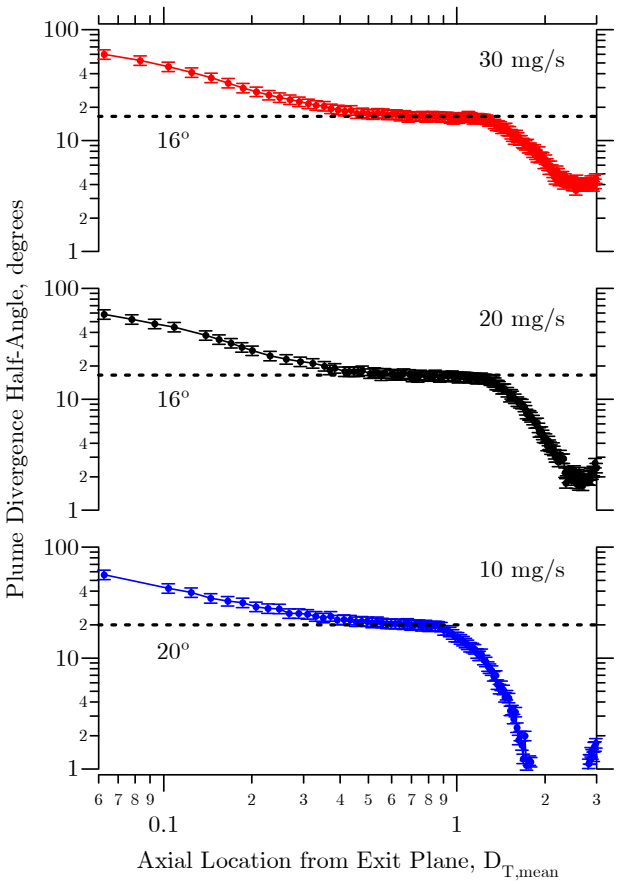

Figure 9 Plume divergence at each axial location for thruster operation at 300 V and 10, 20, and 30 mg/s.

The plume divergence decreased from 10 to 20 mg/s and remained constant from 20 to 30 mg/s. This is consistent with the trend of decreasing plume divergence with flow rate measured with the NASA-173Mv1 [20]. The trend was unexpected for the 6-kW Hall thruster since ion acceleration occurred further downstream as flow rate was increased [13-14]. Typically, moving the acceleration downstream results in higher plume divergence since the electric field becomes defocused outside the channel. However, the 6-kW thruster in this study did not have a defocused potential structure in the very-near-field; hence, a wide range of axial acceleration locations maintained excellent beam collimation and led to a relatively uniform divergence across flow rate.

C. Comparison with Far-field Measurements

Although beam divergence and beam current are often useful for spacecraft integration purposes (protecting solar panels, optics, etc.), the goal of these measurements was to relate these properties to the losses that limit efficiency. Additional probe measurements were combined with the near-field Faraday probe measurements to calculate the anode efficiency using a phenomenological efficiency architecture [1]. The results are shown in Table 1. The calculated efficiency was lower than the measured value by 2, 3, and 4% at 10, 20, and 30 mg/s.

The results from the near-field measurements were compared to traditional far-field measurements recorded at the same thruster conditions. Traditional analysis methods produced beam divergence angles of approximately 49° (η_d = 0.43) and beam currents that were approximately 1.02 I_d. Both of these values are unreasonably large and generate calculated efficiencies of 0.40, 0.38, and 0.37 at 10, 20, and 30 mg/s, respectively. These are very different than the approximately 0.65 anode efficiency measured by a thrust stand. A substantial improvement in results can be realized by analyzing the results with a correction for cosine losses [21]. This method decreases the calculated beam divergence to 27° (η_d = 0.79); however, the current utilization is still greater than 0.9 at all three operating conditions (expected to be approximately 0.8). Although the current utilization is higher than expected, the combined result is that the calculated efficiency matches the near-field values to within a few percent (absolute not

relative). This agreement is coincidence rather than validation of either measurement; the far-field analysis over-predicted both beam divergence and beam current, which counterbalanced each other.

The calculated anode efficiencies from all three methods (near-field, far-field, and far-field) displayed the same decreasing trend with flow rate. This trend did not agree with the slightly positive trend that was shown in thrust stand measurements. The primary contributor to this trend was the decreasing current utilization with flow rate (note that divergence, charge, and voltage utilizations were all nearly constant from 10-30 mg/s). This discrepancy indicates that the near-field results under predicted the beam current as flow rate was increased. The reason for this potential discrepancy in the current utilization trend is not well understood.

Table 1 Comparison of calculated plume divergence, beam current, and anode efficiency for near-field and far-field measurements. The measured anode efficiencies from thrust stand measurements are included for comparison. Values in parentheses indicate utilization efficiencies.

	10 mg/s	20 mg/s	30 mg/s
Near-field			
Plume Divergence	20° (0.884)	16° (0.923)	16° (0.922)
Beam Current, A	7.35 (0.812)	15.8 (0.777)	25.9 (0.766)
Calculated Anode Efficiency, -	0.626	0.613	0.603
Far-field (Cosine Analysis)			
Plume Divergence	27° (0.794)	27° (0.794)	27° (0.794)
Beam Current, A	8.25 (0.911)	18.6 (0.915)	30.4 (0.900)
Calculated Anode Efficiency, -	0.631	0.621	0.609
Far-field (Traditional Analysis)			
Plume Divergence	48° (0.448)	49° (0.430)	49° (0.430)
Beam Current, A	9.23 (1.02)	21.0 (1.03)	34.3 (1.02)
Calculated Anode Efficiency, -	0.398	0.380	0.372
Thrust Stand			
Measured Anode Efficiency, -	0.641	0.645	0.646

Additional measurements were taken at 150 V and 10, 20, and 30 mg/s that also showed reasonably good consistency with thrust stand measurements [2]. The calculated anode efficiency was respectively within 5.1, 4.7, and 6.6% of the measured values (absolute not relative). Combining the low-voltage measurements with those presented at 300 V indicates that the method is applicable across a wide range of voltages and discharge powers (1-10 kW).

V. Conclusions

Near-field Faraday probe measurements were analyzed with a proposed 1/e definition for the beam current integration and beam divergence. The results for both parameters were uniform from approximately 0.5 to 1 $D_{T,mean}$, indicating consistency of the measurement and analysis over a finite region of the plume. Beyond that point, thruster- and facility-induced collisions altered the plume and the resulting calculations of beam current and beam divergence varied significantly. Global values of the beam current and beam divergence were determined from the

average between 0.5 and 1 $D_{T,mean}$ and used to determine the current utilization and divergence utilization, respectively. These utilizations were combined with other probe measurements to calculate the anode efficiency. Although the agreement between the calculated and measured efficiencies was quite good, the decreasing trend of the calculated efficiency with flow rate did not match the constant efficiency measured with the thrust stand. The decreasing trend in current utilization with flow rate was the primary cause for this discrepancy.

The outcome of this work should be used as a baseline for improving beam current and beam divergence measurements. The near-field results in this paper were superior to those from far-field measurements and indicated that radial measurements in the near-field plume combined with the suggested 1/e analysis bounds produced beam current (current utilization) and beam divergence (divergence utilization) values that were consistent with thrust stand measurements from 1 to 10 kW (150 V at 10, 20, and 30 mg/s not presented here).

As a minimum, we recommend that near-field measurements be taken along radial paths from 0 to 2 $D_{T,mean}$ in the radial direction and from 0 to 2 $D_{T,mean}$ in the axial direction. The probe should be moved at high speed to reduce the effects of probe heating and current density measurements should be taken at high speed to adequately resolve discharge current fluctuations and to provide high spatial resolution. Although the suggested measurement technique and analysis methods provided consistent results, they are not proposed as the ultimate solution. Instead, this concept should be investigated in further detail to validate the findings across several thruster designs, operating conditions, and vacuum facilities.

References

1. Hofer, R. R., Katz, I., Mikellides, I. G., Goebel, D. M., Jameson, K. K., Sullivan, R. M., and Johnson, L. K., "Efficacy of Electron Mobility Models in Hybrid-PIC Hall Thruster Simulations," *AIAA/ASME/SAE/ASEE Joint Propulsion Conference*, AIAA-2008-4924, Hartford, CT, Jul. 20-23, 2008.

2. Reid, B. M., "The Influence of Neutral Flow Rate in the Operation of Hall Thrusters," Ph.D. Dissertation, Dept. of Aerospace Engineering, University of Michigan, Ann Arbor, MI, 2009.

3. Hofer, R. R., Jankovsky, R. S., and Gallimore, A. D., "High-Specific Impulse Hall Thrusters, Part 2: Efficiency Analysis," *Journal of Propulsion and Power* Vol. 22, No. 4, 2006, pp. 732-740.

4. Hofer, R. R., and Gallimore, A. D., "Recent Results from Internal and Very-Near-Field Plasma Diagnostics of a High Specific Impulse Hall Thruster," *28th International Electric Propulsion Conference*, IEPC-2003-037, Toulouse, France, Mar. 17-21, 2003.

5. Jameson, K. K., Goebel, D. M., Hofer, R. R., and Watkins, R. M., "Cathode Coupling in Hall Thrusters," *30th International Electric Propulsion Conference*, IEPC-2007-278, Florence, Italy,

6. Walker, M. L. R., "Effects of Facility Backpressure on the Performance and Plume of a Hall Thruster," Dept. of Aerospace Engineering, University of Michigan, Ann Arbor, MI, 2005.

7. Reid, B. M., Shastry, R., Gallimore, A. D., and Hofer, R. R., "Angularly-Resolved ExB Probe Spectra in the Plume of a 6-kW Hall Thruster," *44th AIAA/ASME/SAE/ASEE Joint Propulsion Conference*, AIAA-2008-5287, Hartford, CT, Jul. 20-23, 2008.

8. Haas, J. M., Hofer, R. R., Brown, D. L., Reid, B. M., and Gallimore, A. D., "Design of the ## Hall Thruster for High Thrust/Power Investigation," *54th JANNAF Propulsion Meeting*, Denver, CO, May 14-17, 2007.

9. Reid, B. M., Gallimore, A. D., Hofer, R. R., Li, Y., and Haas, J. M., "Anode Design and Verification for the ## Hall Thruster," *54th JANNAF Propulsion Meeting*, Denver, CO, May 14-17, 2007.

10. Hofer, R. R., Goebel, D. M., and Watkins, R. M., "Compact LaB6 Hollow Cathode for the ## Hall Thruster," *54th JANNAF Propulsion Meeting*, Denver, CO, May 14-17, 2007.

11. Brown, D. L., Reid, B. M., Gallimore, A. D., Hofer, R. R., Haas, J. M., and Larson, C. W., "Performance Characterization and Design Verification of the ## Laboratory Model Hall Thruster," *54th JANNAF Propulsion Meeting*, Denver, CO, May 14-17, 2007.

12. Haas, J. M., Gallimore, A. D., McFall, K., and Spanjers, G., "Development of a High-Speed, Reciprocating Electrostatic Probe System for Hall Thruster Interrogation," *Review of Scientific Instruments* Vol. 71, No. 11, 2000, pp. 4131-4138.

13. Reid, B. M., and Gallimore, A. D., "Langmuir Probe Measurements in the Discharge Channel of a 6-kW Hall Thruster," *44th AIAA/ASME/SAE/ASEE Joint Propulsion Conference*, AIAA-2008-4920, Hartford, CT, Jul. 20-23, 2008.

14. Reid, B. M., and Gallimore, A. D., "Plasma Potential Measurements in the Discharge Channel of a 6-kW Hall Thruster," *44th AIAA/ASME/SAE/ASEE Joint Propulsion Conference*, AIAA-2008-5185, Hartford, CT, Jul. 20-23, 2008.

15. Shastry, R., Hofer, R. R., Reid, B. M., and Gallimore, A. D., "Method for Analyzing ExB Probe Spectra from Hall Thruster Plumes," *44th AIAA/ASME/SAE/ASEE Joint Propulsion Conference*, AIAA-2008-4647, Hartford, CT, Jul. 20-23, 2008.

16. Peterson, P. Y., Gallimore, A. D., and Haas, J. M., "An Experimental Investigation of the Internal Magnetic Field Topography of an Operating Hall Thruster," *Physics of Plasmas* Vol. 9, No. 10, 2002.

17. Randolph, T., Kim, V., Kaufman, H. R., Kozubsky, K., Zhurin, V. V., and Day, M., "Facility Effects on Stationary Plasma Thruster Testing," *23rd International Electric Propulsion Conference*, Seattle, WA, Sept. 13-16, 1993.

18. Smith, T. B., "Deconvolution of Ion Velocity Distributions from Laser-Induced Fluorescence Spectra of Xenon Electrostatic Thruster Plumes," Doctoral, Dept. of Aerospace Engineering, University of Michigan, Ann Arbor, MI, 2003.

19. Huang, D., Reid, B. M., Smith, T. B., and Gallimore, A. D., "Laser-Induced Fluorescence of Singly-Charged Xenon in a 6-kW Hall Thruster Plume," *44th AIAA/ASME/SAE/ASEE Joint Propulsion Conference*, AIAA-2008-5102, Hartford, CT, Jul. 20-23, 2008.

20. Linnell, J. A., and Gallimore, A. D., "Krypton Performance Optimization in High Voltage Hall Thrusters," *Journal of Propulsion and Power* Vol. 22, No. 4, 2006, pp. 921-925.